

A Langevin dynamics approach for multi-layer mass transfer problems

Oded Farago¹ and Giuseppe Pontrelli^{*2}

¹Department of Biomedical Engineering, Ben-Gurion University of the Negev, Be'er Sheva 85105, Israel

²Istituto per le Applicazioni del Calcolo - CNR, Via dei Taurini 19, 00185 Rome, Italy

November 23, 2020

Abstract

We use Langevin dynamics simulations to study the mass diffusion problem across two adjacent porous layers of different transport property. At the interface between the layers, we impose the Kedem-Katchalsky (KK) interfacial boundary condition that is well suited in a general situation. A detailed algorithm for the implementation of the KK interfacial condition in the Langevin dynamics framework is presented. As a case study, we consider a two-layer diffusion model of a drug-eluting stent. The simulation results are compared with those obtained from the solution of the corresponding continuum diffusion equation, and an excellent agreement is shown.

Keywords: composite materials, interface conditions, diffusion equations, mass flux, Langevin dynamics

1 Introduction

Multi-layer diffusion problems arise in a number of applications of heat and mass transfer. Some industrial examples are moisture diffusion in woven fabric composites [1], hydrodynamics of stratified fluids and geological profiles [2], environmental phenomena such as transport of contaminants, chemicals and gases in layered porous media [3], and chamber-based gas fluxes [4]. Numerous applications concern the biomedical field and include, for example, transdermal drug delivery [5], drug-eluting stents [6] or brain tumor growth [7]. While here we focus on multi-layer diffusion, other related concepts such as anomalous diffusion, fractal kinetics and non-homogenous layers, have been also studied within the context of drug release, see e.g., [8, 9, 10].

*Corresponding author. Email: giuseppe.pontrelli@gmail.com

Often, the transported material is initially concentrated in one of the layers from which it propagates to the others by diffusion. The rate of transfer across the system is mainly determined by the diffusion coefficients in each layer. In many practical applications it is essential to regulate the mass flux between layers by suitable interface conditions. This can be accomplished, for instance, by placing a selective barrier between adjacent layers, which induces a chemical potential gradient at the boundary. Another mean for controlling the transfer rate are membranes which are essentially very thin boundary layers with a small diffusion coefficient [11]. In addition to their role in slowing down the diffusion rate, membranes are also employed for specific functions, including separation/purification of gases, vapors, liquids, selection of ions, or other biological functions. Membranes are routinely used for medical care and individual protection, such as wound dressing, dialysis, tissue engineering, and controlled release of drugs. Membranes are also used for environmental cleaning and protection, such as water purification and air filtration. A better understanding of physical behaviour of membranes as rate-controlling barriers can greatly improve the efficiency of separation and enhance their performance [12].

In this work, we consider simple models for mass transfer in multi-layered systems. We assume that the molecules are transported across the boundaries by passive diffusion only, i.e., no active transport process is performed to drive the random motion of molecules. Passive diffusion continues until enough molecules have passed from a region of higher to a region of lower concentration, to make the concentration uniform. When equilibrium is established, the flux of molecules vanishes: the molecules keep moving, but an equal number of them move into and out of both layers. Much work has been done from the analytical and computational point of view for treating multi-layer diffusion in continuum mechanics. An important aspect of layered systems is the matching conditions at the interfaces, where an interface is the common boundary between two layers. Analytical solutions to such problems are highly valuable as they provide a great level of insight into the diffusive dynamics and can be used to benchmark numerical solutions [13]. Various methods are available for the analysis and the solution of such problems [14, 15]: The orthogonal expansion technique and the Green's function approach [16, 17, 18, 19], the adjoint solution technique [20], the Laplace transform method [14, 15, 21, 22, 23], and finite integral transforms [24, 25, 26]. Integral transform techniques applied to heat transfer problems was reported in great detail in the book by Özişik [20], where several different transformations are given depending on the situation. However, there are severe numerical instabilities and computational drawbacks that arise when the number of layers increases [22]. Other papers demonstrate the complexity of solving diffusion problems with a large number of layers, either using eigenfunction expansion for somewhat different boundary conditions [27], or based on the Green function approach with biological applications [28]. Computational complexity of finite difference schemes is widely discussed [29].

Recently, a new computational method for studying diffusion problems in multi-layer systems has been proposed [30, 31]. The method is based on the well-established notion that Brownian dynamics of particles can be also described by the Langevin's equation (LE) [32]. Therefore, the particle's probability distribution function (or, equivalently, the material concentration) can be computed from an ensemble of statistically-independent single particle trajectories generated by numerical integration of the corresponding LE. Integrating LE within each layer is pretty straightforward, and there are a number of algorithms (Langevin "thermostats") that are widely used for molecular dynamics simulations at constant temperature [33, 34, 35]. The key problem is how to

perform the integration during time-steps where the particle moves between layers, in a manner ensuring that the imposed interlayer conditions are satisfied. In Ref. [31], a set of algorithms for handling the dynamics across sharp interfaces has been introduced. Here we present an algorithm that combines many types of interfaces (a sudden change in diffusivity, a semi-permeable membrane, and an imperfect contact), with the advantage of treating all these cases with a unified physical-based method. The new algorithm is applied for studying a two-layer model of drug release from a drug eluting stent into the artery. Excellent agreement is found between the LE computational results and the semi-analytical solution.

2 Multi-layer systems: diffusion equation

Let us consider a composite medium consisting of a number of layered slabs. A slab is defined here as a plate that is homogeneous and isotropic, having a finite thickness, but extends to infinity in the other two dimensions. In a typical diffusion problem driven by concentration gradient, most of the mass dynamics occurs along the direction normal to the layers. We, therefore, restrict our study to a simplified one-dimensional model across a multi-layer system. The concentration of material in each region, $c_i(x, t)$ ($i = 1, \dots, n$), is governed by the time-dependent diffusion equation

$$\frac{\partial c_i}{\partial t} = D_i \frac{\partial^2 c_i}{\partial x^2}, \quad (2.1)$$

where D_i is the diffusion coefficient in the i -th region. The concentrations in the adjacent regions i and $i + 1$ must be matched at the boundary between them, which is located at $x = L_i$. Two interfacial boundary conditions (IBCs) must be specified at each interface. If mass is conserved (no source or sink) at the interface, then the concentration flux must be continuous

$$J_i = -D_i \frac{\partial c_i}{\partial x} = -D_{i+1} \frac{\partial c_{i+1}}{\partial x} = J_{i+1} \quad \text{at } x = L_i, \quad t > 0. \quad (2.2)$$

The other IBC to be specified at $x = L_i$ depends on the nature of the interface. The transport of material can be completely blocked by placing a perfectly reflecting ($J_i = 0$) or perfectly absorbing ($c_i = 0$) barriers. Typically, however, we are interested at intermediate situations where the mass flux is not completely blocked, but only hindered by interfaces whose aim is to control the rate of mass transfer across the layers. Here, we consider Kedem-Katchalsky (KK) IBC that reads [36, 37]

$$J_i = P_i (c_i - \sigma_i c_{i+1}), \quad \text{at } x = L_i, \quad t > 0, \quad (2.3)$$

where P_i and σ_i are, respectively, the permeability and partition coefficients of the KK condition. We focus on the KK IBC (2.3) because it represents the most general case of an interface where both a discontinuity in the chemical potential and a semi-permeable membrane are present, in addition to a possible discontinuity in the diffusion coefficient. The case without a membrane corresponds to the limit $P_i \rightarrow \infty$, when the KK IBC must be replaced with

$$c_i = \sigma_i c_{i+1}, \quad \text{at } x = L_i, \quad t > 0 \quad (2.4)$$

or, otherwise, the flux diverges at the interface. Eq. (2.4) describes the interfacial condition at an imperfect contact boundary with partition coefficient σ_i arising from the discontinuity in the chemical potential of the transported molecules in the adjacent layers [31]. In the special case of Eq. (2.4) when $\sigma_i = 0$ (or, $\sigma_i \rightarrow \infty$), we have $c_i = 0$ (or, $c_{i+1} = 0$), which describes a perfectly absorbing boundary. A subcase of (2.4) is $\sigma_i = 1$ (a *perfect* contact), when the concentration exhibits no discontinuity for $P_i \rightarrow \infty$. However, when P_i is finite in eqn (2.3), we expect a concentration jump even for $\sigma_i = 1$, as the KK IBC reduces to

$$J_i = P_i (c_i - c_{i+1}), \quad \text{at } x = L_i, \quad t > 0, \quad (2.5)$$

which is the IBC describing the effect of a thin semi-permeable membrane with permeability P_i , but without a chemical potential jump. Finally, when $P_i = 0$, we recover the condition at a perfectly reflecting boundary, $J_i = 0$.

3 Multi-layer systems: Langevin equation

The method presented in ref. [31] is based on the description of the overdamped Brownian motion of particles via the underdamped LE

$$m \frac{dv}{dt} = -\alpha(x)v + \beta(t) + f(x), \quad (3.1)$$

where m and $v = dx/dt$ denote, respectively, the mass and velocity of the diffusing particle. This is Newton equation of motion under the action of a “deterministic” force $f(x)$. The impact of the random collisions between the Brownian particle and the molecules of the embedding medium is introduced by two additional forces - (i) a friction force, $-\alpha(x)v$, and (ii) stochastic Gaussian thermal noise, $\beta(t)$, with zero mean, $\langle \beta(t) \rangle = 0$, and delta-function auto-correlation, $\langle \beta(t)\beta(t') \rangle = 2k_B T \alpha(x(t)) \delta(t - t')$, where T is the temperature and k_B is Boltzmann’s constant [38]. The friction coefficient, α , in LE and the diffusion coefficients, D , in the corresponding diffusion equation, satisfy the Einstein’s relation [32, 39]:

$$\alpha(x)D(x) = k_B T. \quad (3.2)$$

In the Langevin dynamics approach to multi-layer diffusion, the concentration profile, $c(x, t)$, is computed by generating an ensemble of statistically-independent particle trajectories of duration t , from which a fine-grained histogram can be constructed. We define $c(x, t)$ such that, at $t = 0$, the total density is normalized to unity and essentially represents the initial probability distribution function of the particles

$$\int_{-\infty}^{\infty} c(x, 0) dx = 1. \quad (3.3)$$

The trajectories are calculated by numerically integrating Eq. (3.1). To allow for simulations of Langevin dynamics in multi-layer systems, algorithms were derived in [31] for handling the transition in presence of (i) layers with different diffusion coefficients, (ii) a semi-permeable membrane, and (iii) a step-function chemical potential. Here, we integrate them into a single unified

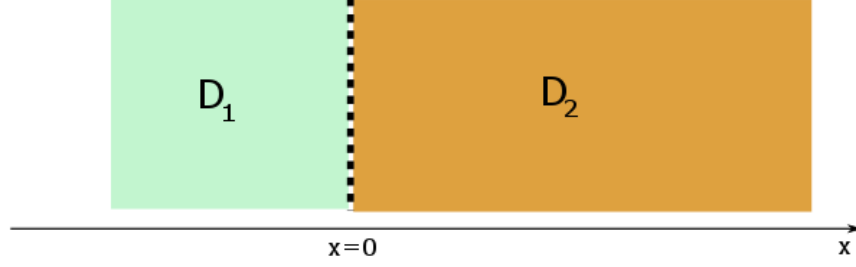


Figure 1: The typical two-layer one-dimensional system. A continuous flux [see Eq. (3.5)] is imposed at the interface $x = 0$ (dashed line), together with Kedem-Khatchalsky (KK) condition [see Eq. (3.6)].

algorithm for crossing a KK IBC [Eq. (2.3)] with continuous flux [IBC Eq. (2.2)]. We will not repeat the discussion on the physical basis underlying the method, but rather present a practical *recipe* describing how to implement the algorithm. To this purpose, we consider the two-layer system shown in fig. 1, with a step diffusion function

$$D(x) = \begin{cases} D_1 & x < 0 \\ D_2 & x > 0. \end{cases} \quad (3.4)$$

The continuity of flux J applies at the interface

$$-D_1 \frac{\partial c_1}{\partial x} = -D_2 \frac{\partial c_2}{\partial x} \quad \text{at } x = 0, \quad t > 0, \quad (3.5)$$

together with the KK IBC

$$J = P(c_1 - \sigma c_2), \quad \text{at } x = 0, \quad t > 0. \quad (3.6)$$

3.1 Langevin integrator

The initial position of the particle is drawn from the probability distribution $c(x, 0)$, Eq. (3.3), and the initial velocity from the Maxwell-Boltzmann distribution

$$\rho_{\text{MB}}(v) = \sqrt{\frac{m}{2\pi k_B T}} \exp\left(-\frac{mv^2}{2k_B T}\right). \quad (3.7)$$

The trajectory $x(t)$ is then computed by performing discrete-time integration of LE (3.1). For this purpose, we use the algorithm of Grønbech-Jensen and Farago (GJF) [35]

$$x^{n+1} = x^n + b \left[dt v^n + \frac{dt^2}{2m} f^n + \frac{dt}{2m} \beta^{n+1} \right] \quad (3.8)$$

$$v^{n+1} = a v^n + \frac{dt}{2m} (a f^n + f^{n+1}) + \frac{b}{m} \beta^{n+1}, \quad (3.9)$$

to advance the coordinate $x^n = x(t_n)$ and velocity $v^n = v(t_n)$ by one time step from $t_n = n dt$ to $t_{n+1} = t_n + dt$. In the above GJF equations (3.8)-(3.9), $f^n = f(x^n)$, β^n is a Gaussian random number satisfying

$$\langle \beta^n \rangle = 0; \quad \langle \beta^n \beta^l \rangle = 2\alpha k_B T dt \delta_{n,l}, \quad (3.10)$$

and the damping coefficients of the algorithm are

$$b = \frac{1}{1 + (\alpha dt/2m)}, \quad a = b [1 - (\alpha dt/2m)]. \quad (3.11)$$

The GJF integrator is chosen because of its robustness against discretization time errors, which is critical for achieving accurate statistics of configurational results. More specifically, it accomplishes statistical accuracy for configurational sampling of the Boltzmann distribution in closed systems; and it also provides the correct Einstein diffusion, $\langle x^2 \rangle = 2(k_B T/\alpha)t$, of a freely diffusing particle in an unbounded system with constant α [35, 40, 41, 42].

We note that Langevin dynamics is diffusive only on time scales larger the so called ballistic crossover time $\tau_{\text{ballistic}} = m/\alpha$, whereas it is predominantly ballistic (inertial) on much smaller time scales. Generally speaking, the GJF integrator can be implemented in simulations with relatively large time steps, $dt > \tau_{\text{ballistic}}$, and still produce accurate statistical results at asymptotically large times [35]. A criterion for choosing dt can be set by the requirement that the characteristic variations in $f(x)$, during the time step, should not be significant, i.e., $|f^{n+1} - f^n| \ll |f^n + f^{n+1}|/2$. This criterion becomes meaningless when a KK interface is crossed because the interface exerts a singular, delta-function, force [31]. Nevertheless, we will demonstrate that an accurate algorithm can be devised provided that the integration is performed in the inertial regime with $dt \ll \tau_{\text{ballistic}}$ (see next section). This implies that the integration time step in multi-layer systems is bounded by the ballistic time at the most viscous medium:

$$dt \ll \tau_{\text{ballistic}}^{\min} = \frac{m}{\max(\alpha_i)} = \min(D_i) \frac{m}{k_B T}. \quad (3.12)$$

3.2 The case of crossing a discontinuity

Before presenting the algorithm for crossing a KK type IBC, the following quantities must be introduced:

- The thermal velocity of the particle, which is independent of α , is given by

$$v_{\text{th}} = 2 \int_0^\infty v \rho_{\text{MB}}(v) dx = \sqrt{\frac{2k_B T}{\pi m}}, \quad (3.13)$$

where $\rho_{\text{MB}}(v)$ is the equilibrium Maxwell-Boltzmann velocity distribution (3.7).

- The crossing probability is related to the membrane permeability P and to the thermal velocity v_{th} by [31]

$$p = \frac{2P}{2P + v_{\text{th}}} \quad (3.14)$$

- At the interface we have a step-function chemical potential¹

$$\phi_{\text{step}} = k_B T \ln(\sigma) H(x), \quad (3.15)$$

where

$$H(x) = \begin{cases} 0 & x < 0 \\ 1 & x > 0 \end{cases} \quad (3.16)$$

is the Heaviside step function. The step-function potential result in a delta-function force $f_{\text{step}} = -d\phi_{\text{step}}/dx = -k_B T \ln(\sigma) \delta(x)$ with a singularity at the interface. In the proposed computational scheme, the singular delta-function force is replaced with a sharp, piecewise constant force

$$f(x) = \begin{cases} -\frac{k_B T \ln(\sigma)}{2\Delta_1} & -\Delta_1 < x < 0 \\ -\frac{k_B T \ln(\sigma)}{2\Delta_2} & 0 < x < \Delta_2 \\ 0 & \text{elsewhere,} \end{cases} \quad (3.17)$$

defined in the "small" interval

$$[-\Delta_1, \Delta_2] = \left[-\frac{\gamma D_1}{v_{th}}, \frac{\gamma D_2}{v_{th}} \right], \quad (3.18)$$

with the associated potential

$$\phi(x) = -\int_{-\infty}^x f(y) dy. \quad (3.19)$$

The thickness of *interface layer* (IL) $[-\Delta_1, \Delta_2]$ over which the chemical potential changes by $k_B T \ln(\sigma)$ is controlled by the dimensionless parameter γ . In the simulations, γ is taken to be of the order of unity such that Δ_i ($i = 1, 2$) is comparable or smaller of the particle mean free path, $l_{\text{MFP}} = 2D_i/v_{th}$, i.e. the characteristic distance traveled by the particle within the ballistic time $\tau_{\text{ballistic}}$. The condition (3.12) guarantees that the discrete-time trajectory does not hop from side to side of the interface, but rather passes across the IL and experiences the influence of the force (3.17).

- We define the weight function

$$W(x) = \exp \left[\frac{\phi(x) - \phi_{\text{step}}(x)}{k_B T} \right]. \quad (3.20)$$

One can easily check that $W(x) = 1$ when $f(x) = 0$.

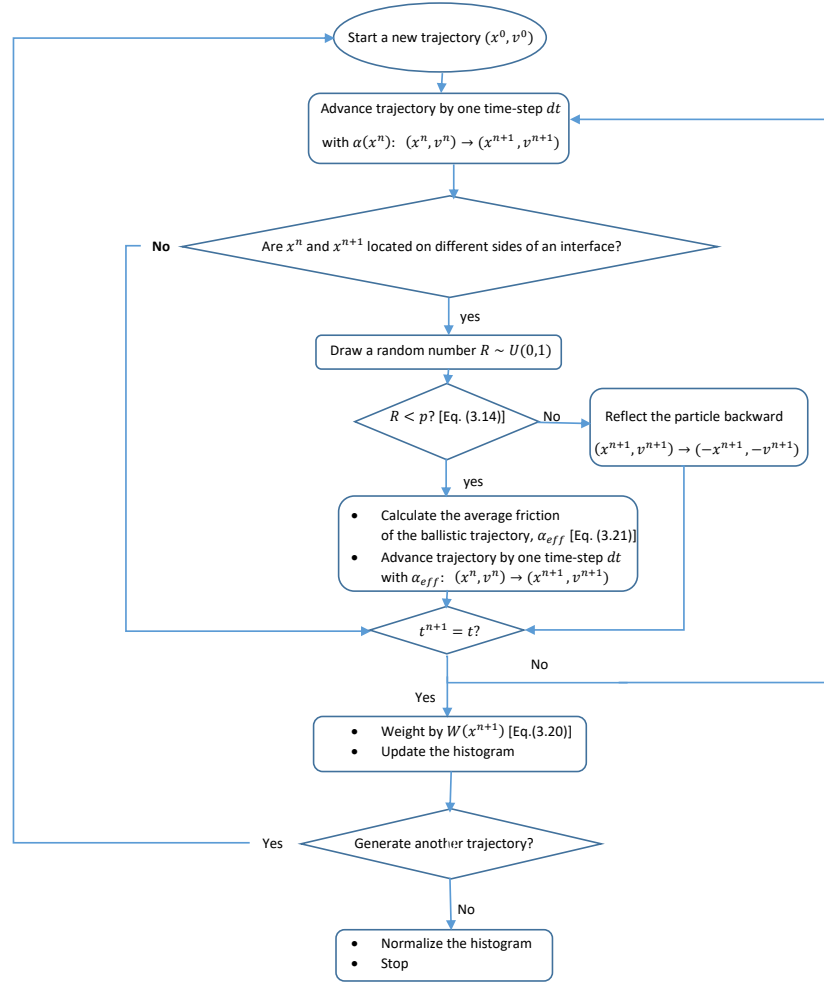


Figure 2: A flowchart representation of the algorithm for Langevin dynamics simulations of a layered system with a KK interface.

With the above in mind, the algorithm for calculating $c(x, t)$ proceeds as follows:

1. Start a new trajectory. Set $t = 0$ and $n = 0$. Choose the initial coordinate x^0 from the initial distribution $c(x, 0)$, and the initial velocity v^0 from the equilibrium Maxwell-Boltzmann velocity distribution (3.7).
2. Advance the trajectory from (x^n, v^n) to (x^{n+1}, v^{n+1}) by one step dt according to Eqs. (3.8)-(3.11), with $f(x)$ given by Eq. (3.17). Use the friction coefficient $\alpha(x^n)$ at $x = x^n$.
3. If x^n and x^{n+1} are found on different sides of the interface then x^{n+1} needs to be recomputed as follows:

¹We exclude the limit cases $\sigma = 0$ and $\sigma \rightarrow \infty$, which correspond to a perfectly absorbing IBC. The transition across such an interface is handled differently, see section 4.

- Choose a random number, \mathcal{R} , uniformly distributed between 0 and 1.
- If $\mathcal{R} > p$ [with p given by Eq. (3.14)], reflect the particle back to the layer from which it arrived and set $(x^{n+1}, v^{n+1}) \rightarrow (-x^{n+1}, -v^{n+1})$
- If $\mathcal{R} < p$, allow the particle to move to the adjacent layer, and determines x^{n+1} as follows:

3.1 Calculate the ballistic position $x_b^{n+1} = x^n + v^n dt$

3.2 Calculate the effective friction coefficient

$$\alpha_{\text{eff}} = \frac{\alpha(x^n) |x^n| + \alpha(x_b^{n+1}) |x_b^{n+1}|}{|x^n| + |x_b^{n+1}|} \quad (3.21)$$

3.3 Advance the trajectory from (x^n, v^n) to (x^{n+1}, v^{n+1}) by one step dt according to Eqs. (3.8)-(3.11), with the effective friction coefficient α_{eff} (3.21). Notice that in some rare cases, the new position x^{n+1} will be found on the same side as x^n , but this is acceptable since small discretization errors are always present when encountering a step function diffusion function.

4. If $t^{n+1} = t$ then

- Stop the trajectory at $x = x^{n+1}$.
- Weight it with the weight function $W(x)$ (3.20), and update the histogram², $\text{hist}_w(x)$, for the distribution function $w(x, t)$: $\text{hist}_w(x) = \text{hist}_w(x) + W(x)$.
- Return to step 1 if you want to generate another trajectory; otherwise go to step 6.

5. Return to step 2.

6. Normalize the distribution, $w(x, t)$, to obtain the concentration profile, $c(x, t)$:

$$c(x, t) = \frac{w(x, t)}{\int_{-\infty}^{\infty} w(x, t) dx}. \quad (3.22)$$

Figure 2 shows a summary of the algorithm in the form of a flowchart.

4 A worked example: a two-layer model of a drug-eluting stent

In this section we consider a biomedical example where the previous concepts and algorithms are applied to a simple model of a drug-eluting stent (DES). Stents are small mesh tubes inserted to keep open stenosed arteries (see fig. 3). Drug-eluting stents (DES) also have an additional thin layer of polymer coating the mesh and eluting a drug. More precisely, a DES is constituted by

²In the histogram representation, $\text{hist}_w(x)$, data accumulate in discrete bins. The continuous distribution $w(x, t)$ is defined as the total value stored within the relevant bin, divided by the bin size.

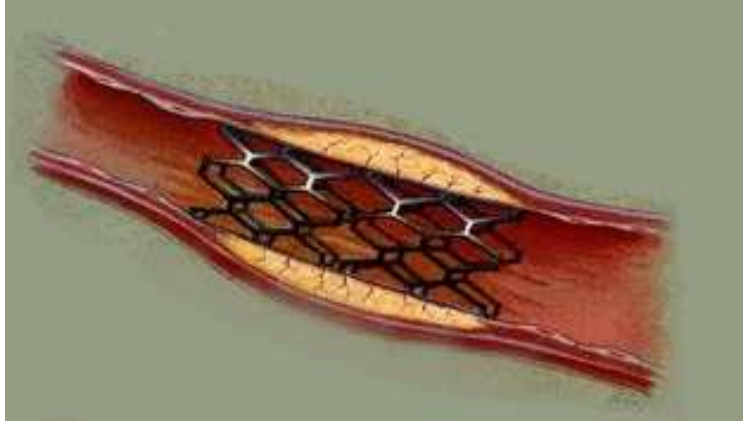


Figure 3: A drug-eluting stent implanted in an artery.

metallic prosthesis (*strut*) implanted into the arterial wall and coated with a thin layer of biocompatible polymer that encapsulates a therapeutic drug (*coating*). Such a drug, released in a controlled manner through a permeable membrane (*topcoat*), is aimed at healing the vascular tissues or at preventing a possible restenosis by virtue of its anti-proliferative action against smooth muscle cells [43, 44].

To formulate the mathematical problem that serves as a simple DES model, let us consider a stent coated by a thin layer (of thickness L_1) of polymer containing a drug and embedded into the arterial wall (of thickness L_2), as illustrated in fig. 4. The complex multi-layered structure of the arterial wall has been disregarded for simplicity, and a homogeneous material with averaged diffusion coefficient D_2 has been considered. A small plasma filtration velocity is present in the wall, but a scaling analysis shows that this transport effect remains negligible in comparison with the diffusive one [43, 47]. The diffusion coefficient of the polymer is $D_1 \ll D_2$. The DES model shown schematically in fig. 4 is a two-layer system similar to the one depicted in fig. 1. The only difference between them is that here the two layers have a finite extent and two boundary conditions (BCs) are prescribed to make the mathematical problem well-posed. Since the strut is impermeable, no mass flux passes through the left boundary surface, which is modelled by imposing a reflecting boundary condition: $J_1(-L_1) = 0$. The right side L_2 , being $L_2 \gg L_1$, is modeled as an absorbing boundary, namely $c_2(L_2) = 0$. At the initial time ($t = 0$), the drug is contained only in the coating (layer 1) and it is uniformly distributed at a maximum concentration C :

$$\begin{aligned} c_1(x, 0) &= C & \text{for } -L_1 \leq x \leq 0 \\ c_2(x, 0) &= 0 & \text{for } 0 \leq x \leq L_2. \end{aligned} \quad (4.1)$$

To slow down the drug release rate, a thin membrane (called *topcoat*) is located at the interface $x = 0$ between the two layers. The topcoat separating the coating and the arterial wall imposes the KK IBC (3.6) between the layers. As no drug is lost in the topcoat, the continuity of the flux IBC (3.5) is also assumed.

To summarize, the two-layer diffusion problem is given by the following set of partial differ-

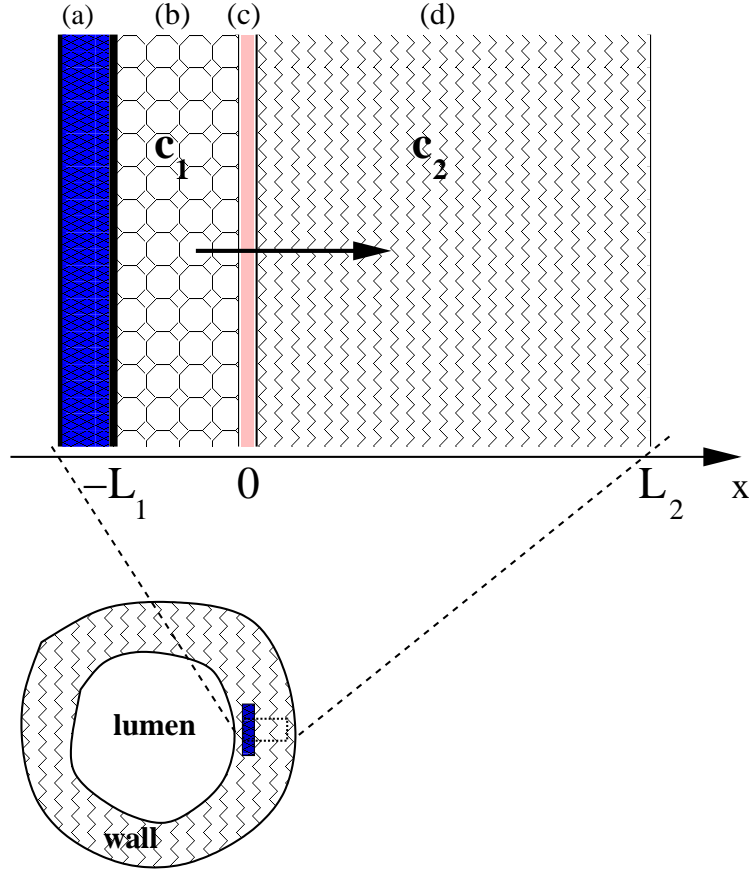


Figure 4: Cross-section of a stented artery with the sequence of layers for drug dynamics (a) stent strut, (b) coating, (c) topcoat, (d) arterial wall (figure not to scale).

ential equations, with boundary and initial conditions [47]:

$$\frac{\partial c_1}{\partial t} - D_1 \frac{\partial^2 c_1}{\partial x^2} = 0 \quad \text{in } [-L_1, 0] \quad (4.2)$$

$$\frac{\partial c_2}{\partial t} - D_2 \frac{\partial^2 c_2}{\partial x^2} = 0 \quad \text{in } [0, L_2] \quad (4.3)$$

$$-D_1 \frac{\partial c_1}{\partial x} = -D_2 \frac{\partial c_2}{\partial x} = P(c_1 - \sigma c_2) \quad \text{at } x = 0 \quad (4.4)$$

$$\frac{\partial c_1}{\partial x} = 0 \quad \text{at } x = -L_1 \quad (4.5)$$

$$c_2 = 0 \quad \text{at } x = L_2 \quad (4.6)$$

$$c_1 = C, \quad c_2 = 0 \quad \text{at } t = 0 \quad (4.7)$$

The solution of the above problem is obtained by separation of variables:

$$c_i(x, t) = X_i(x)G_i(t) \quad i = 1, 2 \quad (4.8)$$

where the spatial functions X_1 and X_2 satisfy the Sturm-Liouville problem:

$$X_1'' = -\lambda_1^2 X_1 \quad \text{in } [-L_1, 0] \quad (4.9)$$

$$X_1' = 0 \quad \text{at } x = -L_1 \quad (4.10)$$

$$D_1 X_1' = D_2 X_2' \quad \text{at } x = 0 \quad (4.11)$$

$$X_2'' = -\lambda_2^2 X_2 \quad \text{in } [0, L_2] \quad (4.12)$$

$$X_2 = 0 \quad \text{at } x = L_2 \quad (4.13)$$

$$-D_2 X_2' + P\sigma X_2 = P X_1 \quad \text{at } x = 0 \quad (4.14)$$

with:

$$D_1 \lambda_1^2 = D_2 \lambda_2^2 \quad (4.15)$$

The general solution of the ordinary differential eqns. (4.9) and (4.12) is:

$$\begin{aligned} X_1(x) &= a_1 \cos(\lambda_1 x) + b_1 \sin(\lambda_1 x) \\ X_2(x) &= a_2 \cos(\lambda_2 x) + b_2 \sin(\lambda_2 x) \end{aligned} \quad (4.16)$$

and

$$G_1(t) = G_2(t) = \exp(-D_1 \lambda_1^2 t) = \exp(-D_2 \lambda_2^2 t) \quad (4.17)$$

The eigenvalues λ_i and the unknown coefficients a_i and b_i are computed by imposing the BCs and IBCs as follows. From (4.10) and (4.13), we have:

$$\begin{aligned} a_1 \sin(\lambda_1 L_1) + b_1 \cos(\lambda_1 L_1) &= 0 \\ a_2 \cos(\lambda_2 L_2) + b_2 \sin(\lambda_2 L_2) &= 0, \end{aligned} \quad (4.18)$$

and from (4.11) and (4.14), it follows that

$$\begin{aligned} D_1 b_1 \lambda_1 &= D_2 b_2 \lambda_2 \\ -D_2 b_2 \lambda_2 + P\sigma a_2 &= P a_1. \end{aligned} \quad (4.19)$$

Eq. (4.18)–(4.19) form a system of four homogeneous linear algebraic equations in the four unknowns a_1, b_1, a_2 and b_2 . To get a non trivial solution, it is needed that the determinant of the coefficient matrix associated with the above system be equal to zero, that is:

$$\tan\left(\sqrt{\frac{D_2}{D_1}} L_1 \lambda_2\right) (D_2 \lambda_2 + P\sigma \tan(\lambda_2 L_2)) - \sqrt{\frac{D_2}{D_1}} P = 0 \quad (4.20)$$

An infinite sequence of eigenvalues $\lambda_{21}, \lambda_{22}, \dots, \lambda_{2m}, \dots$ is obtained as solutions of the above transcendental equation (4.20) (eigencondition). Hence, the complete solution of the problem (4.2)–(4.7) is expressed as a linear superposition of the fundamental solutions:

$$\begin{aligned} c_1(x, t) &= \sum_{m=1}^{\infty} A_m X_{1m}(x) \exp(-D_1 \lambda_{1m}^2 t) \\ c_2(x, t) &= \sum_{m=1}^{\infty} A_m X_{2m}(x) \exp(-D_2 \lambda_{2m}^2 t) \end{aligned} \quad (4.21)$$

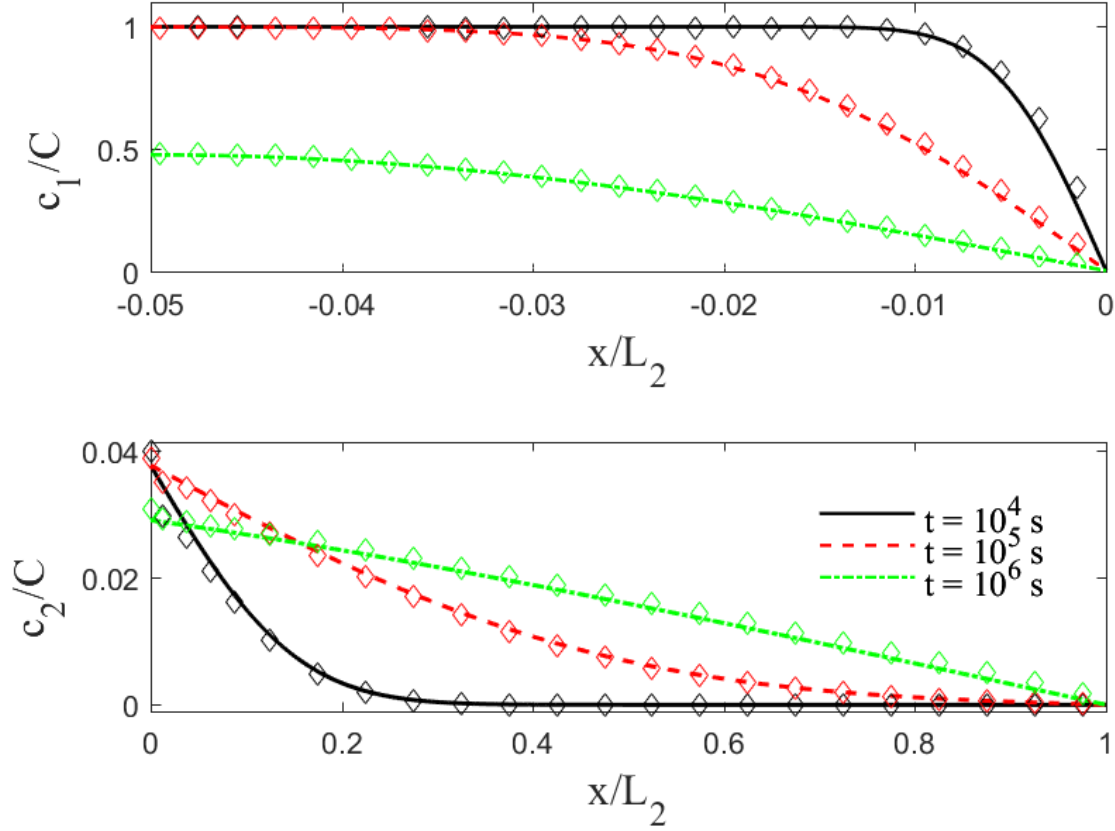


Figure 5: Drug concentration profiles in the coating (above) and in the wall (below) for three times (note the different space scales). The curves depict the solution obtained by separation of variables in [47], while the markers represent the results of the Langevin simulations based on the algorithm described in section 3.2.

where A_m are determined through the initial conditions (4.7) (see [47] for further details).

5 Results

In the absence of direct experiments, we have chosen the following parameters which are in the correct range and for which the resulting release times are consistent with published data [44, 45, 46]:

$$\begin{aligned}
 L_1 &= 5 \cdot 10^{-4} \text{ cm} & L_2 &= 10^{-2} \text{ cm} & D_1 &= 10^{-13} \text{ cm}^2/\text{s} & D_2 &= 7 \cdot 10^{-11} \text{ cm}^2/\text{s} \\
 P &= 10^{-5} \text{ cm/s} & \sigma &= 0.164
 \end{aligned}
 \tag{5.22}$$

These parameters, which are representative of the typical scales in DES, have been chosen based on data in literature for the arterial wall and heparin drug in the coating layer. The same parameters were used in ref. [47], with the exception of D_1 and D_2 have been taken 10^3 smaller, in order to

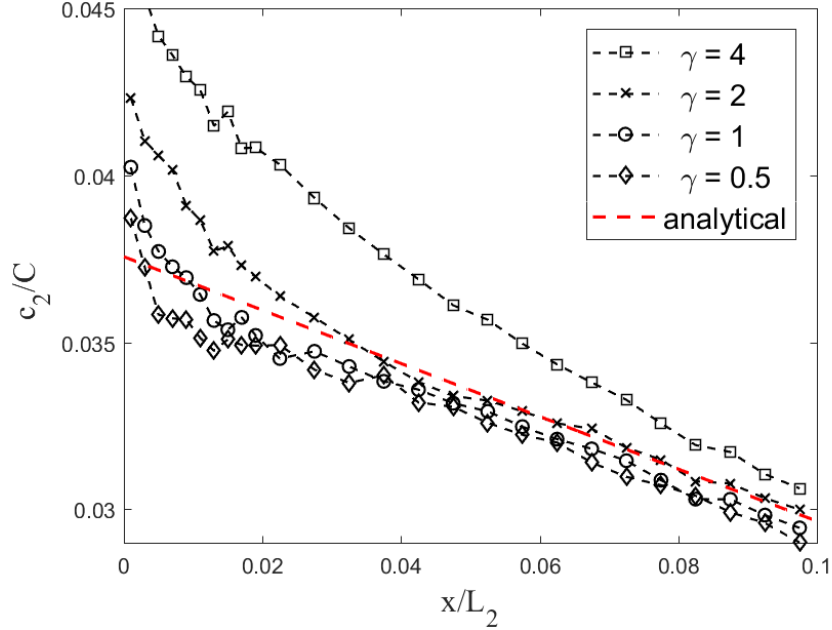


Figure 6: The concentration c_2 at $t = 10^5$ in the region close to the interface. The markers depict the Langevin simulation results with different value of γ in Eq. (3.18), while the dashed red line presents the analytical solution in the limit $\gamma \rightarrow 0$, when the chemical potential is given by a step-function - see Eq. (3.15).

have more realistic release times. For the Langevin simulations, we use dimensionless units with $k_B T = 1$, $v_{th} = 2.523$, $m = 10^{-1}$, $L_1 = 5$, $L_2 = 100$, $D_1 = 10^{-2}$, $D_2 = 7$. For $\gamma = 0.5$ in Eq. (3.18), $\Delta_1 \simeq 2 \cdot 10^{-3} \ll L_1$ and $\Delta_2 = 1.387 \ll L_2$. In these units, $P = 10^{-1}$. Converting the dimensionless units to physical ones, we find that $t = 1$ in the simulations corresponds to $10^3 s$. The time step is set to $5 \cdot 10^{-5}$, which falls in the ballistic regime of the Langevin dynamics in both layers, $\tau_{ballistic}^{\min} = 10^{-3}$ [see Eq. (3.12)]. We note that the reflecting boundary at $x = -L_1$ is treated as special cases of the KK condition with $P = 0$ and $\sigma = 1$ and is, therefore, covered by the above algorithm. The absorbing boundary at $x = L_2$ corresponds to $P \rightarrow \infty$ and $\sigma \rightarrow \infty$ (or $\sigma = 0$). In this case, one should assign a very large (or nearly vanishing) value for σ in Eq. (3.17). In our simulations we use a simpler approach: We do not introduce a force near the absorbing interface and, instead, simply terminate and assign zero weight to each trajectory exceeding L_2 .

The concentration profiles, c_1 and c_2 , for three values of time are displayed in fig. 5. We observe that the concentration c_1 decays in time, indicating that drug is eluting from coating to the wall. The concentration at the wall, c_2 , increases at short times, and decays at longer times as more and more drug arrives at the absorbing surface $x = L_2$. At $x = 0$, where the KK IBC is imposed, we observe a sharp discontinuity in the concentration that diminishes with time. The agreement between the semi-analytical solution (continuous curves) and the Langevin simulation results (diamond symbols) is excellent, except for deviations near $x = 0$ at the shorter time $t = 10^4 s$. These arise from the approximation of the delta-function force at the KK interface by the sharp continuous force (3.17) existing around the interface. The impact of this approximation on the results are supposedly corrected by the weight function

(3.20); however, this correction is based on the ratio of the corresponding Boltzmann factors and, thus, relies on the assumption that locally the system is at thermal equilibrium which, strictly speaking, can be only assumed in the overdamped limit $\tau_{\text{ballistic}} \rightarrow 0$. Fig. 6 presents results for c_2 at $t = 10^5$ with larger values of γ , zooming in on the region close to the interface. The difference between the analytical and numerical solution at $x = 0$ provides a measure of the computational error, Er . Not surprisingly, we find that it decreases almost linearly with γ ($\gamma = 4 : Er = 0.0095$, $\gamma = 2 : Er = 0.0048$, $\gamma = 1 : Er = 0.0028$, $\gamma = 0.5 : Er = 0.0012$) suggesting that the simulations should be run with the smallest possible γ . Nevertheless, γ cannot be reduced indefinitely since the condition $dt \ll \gamma l_{\text{MFP}}/2v_{\text{th}}$ is required to ensure that the particle travels within the IL³.

6 Analysis of discretization errors

In the last section, we have examined the computational error arising from the approximation of a discontinuous chemical potential with a sharp piecewise constant jump. Here, we further expand our analysis, focusing on the convergence and accuracy of the algorithm with respect to the integration time step dt . As noted above, we use the GJF equations (3.8)-(3.11) to integrate the Langevin dynamics, where an ensemble of particle starting on one side of the interface and spreading across the system. We chose this integrator because it yields the correct Einstein diffusion, $\langle x^2 \rangle = 2Dt = 2(k_B T/\alpha)t$, for any time step when applied in simulations of a freely diffusing particle. Thus, the algorithm samples correctly the diffusive dynamics away from the interface, and discretization errors arise from the segments of the trajectories when the particle passes close to the interface. These errors can be minimized by using smaller dt , but that would come at the cost of being able to simulate a smaller number of trajectories per CPU time, which would increase the statistical noise. In order to analyze the convergence of the numerical method with respect to dt , we repeat the simulations of a system with IL parameter $\gamma = 0.5$ for a sequence of decreasing time steps dt_k ($k = 0, 1, 2, \dots$). As a reference case, we set $dt_0 = 25 \cdot 10^{-4}$ which is 50 times larger than the minimal time step dt used to generate the results in fig. 5 and 2.5 times larger than the ballistic time, as computed from Eq. (3.12). We quantify the *distance* between the concentration profiles $c^{(k)}$ corresponding to subsequent time-steps through the Euclidean norm

$$E^k(\cdot, t) = \left\| \frac{c^{(k)} - c^{(k-1)}}{c^{(k)}} \right\|_2, \quad k = 1, \dots, 5 \quad (6.23)$$

The results of the analysis are summarized in table 1. The table shows a clear convergence at smaller time steps and indicates that choosing $dt = 5 \cdot 10^{-5}$ for the simulation results in fig. 5 yields a satisfactory accurate solution. The significant drop in E^k between $k = 2$ and $k = 3$ is probably due to the fact that dt_2 is not sufficiently smaller compared to the ballistic time ($dt_2 = 5 \cdot 10^{-4} = \tau_{\text{ballistic}}/2$). Thus, for the smaller k values in the table the error is predominantly a systematic discretization one, while for the larger values of k is dominated by statistical noise.

³Note that the above condition can be also written as $dt \ll \gamma(\pi/2)\tau_{\text{ballistic}}$, with $\tau_{\text{ballistic}}$ given by Eq. (3.12), which explains why γ should be of the order of unity.

Case	Time step	$E(\cdot, 10^4)$	$E(\cdot, 10^5)$	$E(\cdot, 10^6)$
1	$dt_1 = 20 dt$	0.0138	0.0083	0.0080
2	$dt_2 = 10 dt$	0.0120	0.0142	0.0386
3	$dt_3 = 5 dt$	0.0067	0.0069	0.0074
4	$dt_4 = 2 dt$	0.0051	0.0043	0.0085
5	$dt_5 = dt$	0.0025	0.0024	0.0057

Table 1: Norm of the profile difference at three times for a sequence of decreasing time steps dt_k .

To summarize, the simulation results shown in fig. 5 represents an acceptable compromise between accuracy and computational efficiency, dictated by the available CPU time, the high aspect ratio ($L_2/L_1 = 20$), and the large diffusivity contrast ($D_2/D_1 = 700$).

7 Conclusions and perspectives

We proposed an algorithm for Langevin dynamics simulations in diffusive multi-layer systems, with flux continuity and KK interface condition separating regions of different diffusivity. The proposed method is based on accumulating statistics from a large number of independent single particle trajectories. These are produced by a Langevin dynamics discrete-time integrator, and the proposed algorithm describes how the integration is set up when the particle crosses an interface. From the ensemble of Langevin dynamics trajectories, we generate a fine-grained histogram of the concentration profile that solves the corresponding continuum diffusion equation.

To validate the algorithm, we consider the case study of two-layer model for a DES that can be solved semi-analytically by separation of variables. The agreement between this solution and our computational results is shown to be very good. We also use this example to assess the accuracy and stability of the method. Our analysis suggests that two parameters of the simulations need to be carefully chosen: (i) The integration time step that must be smaller than the ballistic time of the Langevin dynamics, and (ii) the width of the interface layer over which the step-function potential energy is approximated. Reducing the values of these parameters improves the accuracy of the results, but also increases the computational cost since more iterations are needed for generating each trajectory. A careful choice should balance between these two aspects, and depends on the problem in question and on the available computational resources.

While the example discussed here concerns a two-layer system, it should be stressed that a clear advantage of the Langevin dynamics algorithm is in dealing with multi-layer systems that have relevance to applications in many scientific and engineering disciplines. The method can be straightforwardly generalized to any number of interfaces, simply by employing the algorithm whenever a trajectory encounters one of the interfaces. The simplicity of the algorithm is in contrast to analytical solutions that, in general, become increasingly complex and computationally inefficient with larger number of layers. In a future work we plan to present studies of multi-layered systems to demonstrate this important feature of the method.

Another direction is to extend the method to two- and three-dimensional composite systems.

We also intend to consider examples where other mechanisms besides passive diffusion, e.g. advection and mass degradation, are included. For the specific application of drug-eluting stent considered herein, additional efforts are needed to assess and evaluating the relative influence of the various factors, including material properties.

Acknowledgments

Funding from the European Research Council under the European Unions Horizon 2020 Framework Programme (No. FP/2014-2020)/ERC Grant Agreement No. 739964 (COPMAT) is acknowledged.

References

- [1] R. Pasupuleti, Y. Wang, I. Shabalin, L.Y. Li, Z. Liu, S. Grove, Modelling of moisture diffusion in multilayer woven fabric composites, *Comput. Mater. Sci.* 50 (2011), 1675-1680.
- [2] P. Gossel, F. Depasse, Alternating heat diffusion in thermophysical depth profiles: multi-layer and continuous descriptions, *J. Phys. D: Applied Physics* 31 (1998), 216-223.
- [3] G. Liu, B. C. Si, Analytical modeling of one-dimensional diffusion in layered systems with position-dependent diffusion coefficients, *Adv. Water Res.* 31 (2008), 251-268.
- [4] G. Liu, B.C. Si, Multi-layer diffusion model and error analysis applied to chamber-based gas fluxes measurements, *Agricultural Forest Meteorol.* 149 (2009), 169-178.
- [5] G. Pontrelli, F. de Monte, A two-phase two-layer model for transdermal drug delivery and percutaneous absorption, *Math. Biosci.* 257 (2014), 96-103.
- [6] S. McGinty, G. Pontrelli, A general model of coupled drug release and tissue absorption for drug delivery devices, *J. Contr. Release* 217 (2015), 327-336.
- [7] D. Mantzavinos, M. G. Papadomanolaki, Y. G. Saridakis, A. G. Sifalakis, Fokas transform method for a brain tumor invasion model with heterogeneous diffusion in 1+1 dimensions, *Appl. Num. Math.* 104 (2016), 47-61.
- [8] D. Copot, R. L. Magin, R. De Keyser, C. Ionescu, Data-driven modelling of drug tissue trapping using anomalous kinetics, *Chaos, Solitons & Fractals* 102, (2017) 441-446.
- [9] N. Pippa, A. Dokoumetzidis, C. Demetzos, P. Macheras, On the ubiquitous presence of fractals and fractal concepts in pharmaceutical sciences: A Review, *Int. J. Pharmaceutics* 456, (2013), 340-352.

- [10] A. Dokoumetzidis, K. Kosmidis, P. Macheras, Monte Carlo simulations and fractional kinetics considerations for the Higuchi Equation (2011) *Int. J. Pharmaceutics* 418, (2011) 100-103.
- [11] E. L. Cussler, *Diffusion: Mass transfer in fluid systems*, Cambridge University Press, Cambridge, 2009.
- [12] Z. Yao, M. Le Maguer, Mathematical modelling and simulation of mass transfer in osmotic dehydration processes. Part I: Conceptual and mathematical models, *J. Food Engin.* 29 (1996), 349-360.
- [13] E. J. Carr, N. G. March, Semi-analytical solution of multilayer diffusion problems with time-varying boundary conditions and general interface conditions, *Appl Math. Comp.* 333 (2018), 286-303.
- [14] J. Crank, *The Mathematics of Diffusion*, Clarendon Press, Oxford, 1975.
- [15] H. S. Carslaw, J. C. Jaeger, *Conduction of Heat in Solids*, Oxford Press, Oxford, 1959.
- [16] C. W. Tittle, Boundary value problems in composite media: Quasi-orthogonal functions, *J. Appl. Phys.* 36 (1965), 1486-1488.
- [17] G. P. Mulholland, M. H. Cobble, Diffusion through composite media, *Int. J. Heat Mass Transfer* 15 (1972), 147-160.
- [18] W. P. Reid, Heat flow in composite slab, cylinder and sphere, *J. Franklin Inst.* 274 (1962), 352-357.
- [19] D. Ramkrishna, N. R. Amundson, Transport in composite materials: reduction to a self-adjoint formalism, *Chem. Eng. Sci.* 29 (1974), 1457-1464.
- [20] M.N. Özışik, *Heat Conduction*, John Wiley, New York, 1980.
- [21] A. V. Luikov, *Analytical Heat Diffusion Theory*, Academic Press, New York, 1968.
- [22] E.J. Carr, I.W. Turner, A semi-analytical solution for multilayer diffusion in a composite medium consisting of a large number of layers, *Appl. Math. Model.* 40 (2016), 7034-7050.
- [23] E. J. Carr, G. Pontrelli, Modelling mass diffusion for a multi-layer sphere immersed in a semi-infinite medium: application to drug delivery, *Math. Biosci.*, 303 (2018), 1-9.
- [24] N. Y. Ölçer, A general class of unsteady heat flow problems in a finite hollow circular cylinder, *Q. Appl. Math.* 26 (1968), 355-371.
- [25] M. D. Mikhailov, General solutions of the diffusion equations coupled at the boundary conditions, *Int. J. Heat Mass Transfer* 16 (1973), 2155-2164.
- [26] J. Padovan, Generalized Sturm-Liouville procedure for composite domain anisotropic transient conduction problems, *AIAA J.* 12 (1974), 1158-1160.

- [27] F. Martelli, A. Sassaroli, S. Del Bianco, Y. Yamada, G. Zaccanti, Solution of the time-dependent diffusion equation for layered diffusive media by the eigenfunction method, *Phys. Rev. E* 67, (2003), 056623.
- [28] X. Wang, The diffusion equation in multilayered rectangular biological tissue with finite thickness, *Optik* 180 (2019), 144-150.
- [29] R.I. Hickson, S.I. Barry, G.N. Mercer, H.S. Sidhu, Finite difference schemes for multilayer diffusion *Math. Comput. Modelling*, 54 (12) (2011), 210-220.
- [30] S. Regev, O. Farago, Application of underdamped Langevin dynamics simulations for the study of diffusion from a drug-eluting stent, *Physica A: Statistical Mechanics and its Applications* 507 (2018), 231-239.
- [31] O. Farago, Algorithms for Brownian dynamics across discontinuities, [arXiv:2003.09685](https://arxiv.org/abs/2003.09685)v1, submitted to *J. Comput. Phys.* (2020).
- [32] N. G. van Kampen, *Stochastic Processes in Physics and Chemistry*, North-Holland, Amsterdam, 1981.
- [33] A. Brünger, C. L. Brooks, M. Karplus, Stochastic boundary conditions for molecular dynamics simulations of ST2 water, *J. Phys. Lett.* 105 (1984), 495-500.
- [34] B. Leimkuhler, C. Matthews, Rational construction of stochastic numerical methods for molecular sampling, *Applied Mathematics Research Express* 1 (2013), 34-56.
- [35] N. Grønbech-Jensen, O. Farago, A simple and effective Verlet-type algorithm for simulating Langevin dynamics, *Mol. Phys.* 111 (2013), 983-991.
- [36] O. Kedem, A. Katchalsky, Thermodynamic analysis of the permeability of biological membrane to non-electrolytes, *Biochim. Biophys. Acta* 27 (1958), 229-246.
- [37] A. Kargol, M. Kargol, S. Przystalski, The Kedem-Katchalsky equations as applied for describing substance transport across biological membranes, *Cell. Molec. Biol. Lett.* 2 (1996), 117-124.
- [38] H. Risken, *The Focke-Planck Equation*, Springer-Verlag, Berlin, 1988.
- [39] O. Farago, N. Grønbech-Jensen, Fluctuation-dissipation relation for systems with spatially varying friction, *J. Stat. Phys.* 156 (2014), 1093-1110.
- [40] N. Grønbech-Jensen, N. R. Hayre, O. Farago, Application of the G-JF discrete-time thermostat for fast and accurate molecular simulations, *Comput. Phys. Commun.* 185 (2014), 524-527.
- [41] E. Arad, O. Farago, N. Grønbech-Jensen, The G-JF thermostat for accurate configurational sampling in soft-matter simulations, *Isr. J. Chem.* 56 (2016), 629-635.

- [42] J. Finkelstein, G. Fiorin, B. Seibold, Comparison of modern Langevin integrators for simulations of coarse-grained polymer melts, *Mol. Phys.* (2019). <https://doi.org/10.1080/00268976.2019.1649493>
- [43] S. McGinty, A decade of modelling drug release from arterial stents, *Math. Biosci.* 257, (2014), 80-90.
- [44] R. Piccolo, K.H. Bonaa, O. Efthimiou, et. al, Drug-eluting or bare-metal stents for percutaneous coronary intervention: a systematic review and individual patient data meta-analysis of randomised clinical trials, *The Lancet* 393 (2019), 2503-2510.
- [45] C. Hwang, D. Wu, E. R. Edelman, Physiological transport forces govern drug distribution for stent-based delivery, *Circulation* 104 (2001), 600-605.
- [46] D. V. Sakharov, L. V. Kalachev, D. C. Rijken, Numerical simulation of local pharmacokinetics of a drug after intravascular delivery with an eluting stent, *J. Drug Target* 10 (2002), 507-513.
- [47] G. Pontrelli, F. de Monte, Mass diffusion through two-layer porous media: an application to the drug-eluting stent, *Int. J. Heat Mass Transfer*, 50 (2007), 3658-3669.